Remote Sensing for Environmental Monitoring and Change Detection (Proceedings of Symposium HS3007 at IUGG2007, Perugia, July 2007). IAHS Publ. 316, 2007.

MODIS-based estimates of the regional evapotranspiration

RONGLIN TANG[1], JUN XIA[1,2], XIANG ZHANG[1] & XIONGRUI YIN[1]

1 *State Key Laboratory of Water Resources and Hydropower Engineering Science, Wuhan University, Wuhan 430072, China*
trl_wd@163.com

2 *Key Lab. of Water Cycle & Related Surface Processes, Institute of Geographic Sciences and Natural Resources Research, Chinese Academy of Science, Bejing 100101, China*

Abstract The spatial distribution of the regional MODIS-based evapotranspiration (ET) based on surface energy balance and DEM (Digital Elevation Model) and limited weather data is presented. Considering the remotely-sensed sun radiation is higher than actual sun radiation, two calibration factors are introduced with the measured ET, and the results are validated when the instantaneous ET is converted to the diurnal ET. In the process of calibration and validation, the mean value of 3 × 3 pixels, including the observed "point" value, is calculated as the "pixel" value to fit the remotely sensed pixel value to improve the representation of the observed "point" data. At the end of this paper, some common existing concerns are considered and analysed, and some suggestions are put forward.

Key words calibration factors; DEM; evapotranspiration; MODIS

INTRODUCTION

Many approaches based on energy balance have been developed to calculate the evapotranspiration (ET) at basin scale, such as SEBAL (Surface Energy Balance Algorithm for Land, Bastiaanssen, 1995), SEBS (Surface Energy Balance System, Su, 2002), RESEP (Regional Evapotranspiration through Surface Energy Partitioning, Ambast, 2002), etc. Significant progress has also been made in the accuracy of remote sensing models in the calculation of regional ET using both imagery and meteorological data. Initially, the surface ET is divided into soil evaporation and vegetation transpiration (Mo *et al*., 2004) from the one-layered model (the land surface is seen as a uniform surface) to the present two or multi-layered model (the land surface is seen as soil pixel and vegetation pixel). This paper mainly presents the calculation of the surface ET in the Huai River basin, based on energy balance equations using MODIS (Moderate Resolution Imaging Spectroradiometer) imagery, meteorological data, and DEM (Digital Elevation Model) data which outline the changes of the terrain. To match the remotely sensed ET with the point observed ET, a sinusoidal relationship was adopted to calculate the spatial distribution of the diurnal ET in the study area and then perform spatial interpolation of the point observed ET using IDW, Inverse Distance Weighting). The mean value of a 3 × 3 pixel area, including the observed "point" value is calculated as the "pixel" value for comparison with the observed point data. Finally, other observed data precluding the verified aforementioned was used to validate the remotely sensed ET in the study area.

RATIONALE

Surface energy balance

According to the surface energy balance equation, the calculation of the regional ET can be expressed as follows:

$$LE = R_n - H - G \tag{1}$$

where LE is the latent heat flux, R_n is the net radiation, H is the sensible heat flux and G denotes the soil heat flux (all in W m^{-2}). The storage of heat in the plant tissue or volume of canopy and the energy consumption of photosynthesis are negligible compared to the above four fluxes, so they are not considered in this paper. The surface energy components were calculated as follows.

Surface net radiation (R_n)

Surface net radiation can be calculated according to the following two equations:

$$R_n = Q(1 - r_0) + \varepsilon L_{in} - L_{out} \tag{2}$$

$$R_n = Q(1 - r_0) + \varepsilon\sigma(\varepsilon_a T_a^4 - T_s^4) \tag{3}$$

where Q is the downward solar radiation, L_{in} is downward long-wave radiation, L_{out} is upward long-wave radiation (all in W m^{-2}), r_0 is surface albedo, σ is the Stefan-Boltzmann constant (W m^{-2} K^{-4}), T_a is air temperature (K), T_s is land surface temperature (K), ε is land surface emissivity, ε_a is air effective emissivity.

Soil heat flux (G)

Soil heat flux is generally considered as a fraction of the net radiation R_n when it is estimated with remote sensing models:

$$\Gamma = G / R_n \tag{4}$$

As the radiation and energy transfer of plant canopies and soil changes with different surface land cover, Choudhury *et al*. (1984) introduced a proportionality factor Γ to describe the conductive heat transfer in soil and an extinction factor Γ to describe the attenuation of radiation through canopies. As for mixed land surfaces, the fraction can be expressed as follows:

$$\Gamma = G/R_n = \Gamma'\Gamma'' \tag{5}$$

According to studies using SEBAL (Bastiaanssen, 1998), Γ' and Γ'' are closely related to land surface temperature, T_s, land surface albedo, r_0, and Normalized Difference Vegetation Index, *NDVI*:

$$\begin{cases} \Gamma' = T_0(0.0032r_0 + 0.0062(r_0)^2)/r_0 \\ \Gamma'' = 1 - 0.978NDVI^4 \end{cases} \quad (6)$$

The coefficients in the above formulas may change with different patterns of land cover, and the ratio, G/R_n can be expressed according to:

$$\Gamma = \Gamma'\Gamma'' = T_0(t)(0.0032r_0^{avg} + 0.0062(r_0^{avg})^2)(1 - 0.978NDVI^4)/r_0(t) \quad (7)$$

Sensible heat flux (*H*)

The calculation of *H* is the most complex of the four components of the surface energy balance equation and it is associated with the terrain, vegetation height, weather condition and so on. *H* is mainly used to heat up the air above the ground.

$$H = \rho C_p \delta T / r_a = \rho C_p (a + bT_s)/r_{ah} \quad (8)$$

where ρ is air density (kg m^{-3}) C_p is specific heat capacity of air (kJ (kg °C)$^{-1}$), δT is air temperature difference near the surface (°C), r_{ah} is aerodynamic resistance (sm^{-1}), and *a* and *b* are empirical coefficients.

The coefficients *a* and *b* are determined by two "anchor" points in the thermal infrared image, the driest (warmest) point and the wettest (coldest) point. The driest point denotes the very dry bare soil with no or little ET ($H = R_n - G$) while the wettest point denotes the pixel having the maximum ET with sufficient water supply and dense vegetation ($LE = R_n - G$). The coefficients are derived by setting up the linear function of near surface air temperature with the calculated δT at two anchor points.

The determination of r_{ah} is the most significant and complicated in the above equations. Liu *et al*. (2006) described various theories and models that calculate r_{ah}. This paper introduces the Monin-Obukhov similarity theory (Xiaofeng *et al*., 2005) and solves r_{ah} iteratively. A basic assumption in this application is that the Monin-Obukhov length *L* is presumed to be 1000 (a larger number). In this case, the wind speed of every pixel will not be affected by the surface roughness length, and the friction velocity u^* and r_{ah} ($\Psi_h = 0$, $\Psi_m = 0$) can be solved by:

$$\begin{cases} u^* = k * u / \ln((Z-d)/Z_{om}) \\ r_{ah} = \ln((Z-d)/Z_{om}) \ln((Z-d)/Z_{oh}) / (k^2 * u) \end{cases} \quad (9)$$

Based on the assumption proposed in the first step, the δT of the two anchor point (pixels) will be calculated, and then the coefficients, *a* and *b*, will be solved through the linear relationship of δT and T_s. Finally, *H* will be obtained according to equation (8).

The parameters, u^*, Z_{om} and Z_{oh} will be calculated under different atmospheric conditions based on the Monin-Obukhov similarity theory and the equations (8)–(9). In this procedure, *H* will be calculated iteratively until it is stable.

R_n, *G* and *H* can be solved sequentially, via the approaches described earlier, and *LE* can be obtained as the residual of the energy balance equation. The diurnal ET at the study area can also be mapped by the temporal scaling-up (the instantaneous ET is converted to the diurnal ET).

Diurnal ET (E_d)

The instantaneous spatial distribution of the study area at the satellite overpass time can be obtained based on the above-mentioned theory and related remotely sensed inversion of land surface parameters (T_s, r_0, ε, *NDVI*) as well as meteorological inputs. In order to convert the instantaneous values of ET to daily ET values, a sinusoidal relationship between the diurnal ET and the instantaneous ET was used as follows (Xie, 1991):

$$E_d / E_t = 2N_E /(\pi \bullet \sin(\pi t / N_E)) \quad (10)$$

where E_d is the diurnal ET, E_t is the instantaneous ET at the satellite overpass time (both in mm d^{-1}), N_E is the duration of E_d, generally being taken as 2 hours less than sunshine time (h), t is the difference between the satellite overpass time and the time ET starts at (h).

To eliminate the overestimation of the sun's radiation in the morning and afternoon by equation (10) (Wang *et al*., 2002), the spatial E_d distribution is firstly mapped according to equation (10), then some point observations are used to calibrate the corresponding remotely sensed ET, and finally the validation of the calibrated remotely sensed ET is performed. The calibration formula can be expressed as:

$$E_d / E_t = \alpha(2N_E /(\pi \bullet \sin(\pi t / N_E)))^{\beta} \quad (11)$$

where α and β are calibration parameters, reflecting the effects of latitude, sun declination, horizontal advection and cloud cover on the sun radiation.

STUDY AREA AND DATA PREPROCESSING

The study area is located within 111°55′–122°45′E, 30°55′–38°20′N with an area of 270 000 km^2 (Fig. 1). One third of the study area is primarily distributed in the

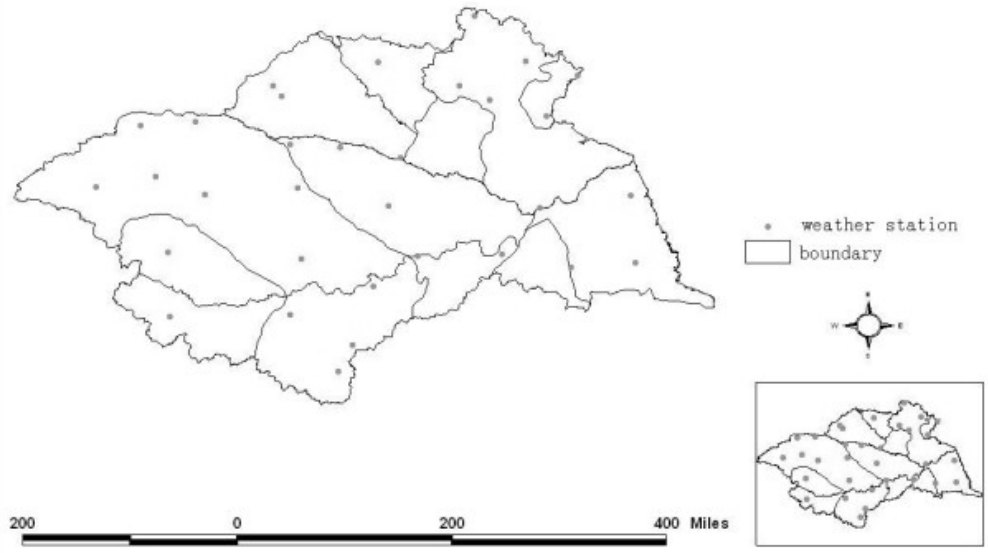

Fig. 1 Meteorological stations in the study area.

western, southwestern and northeastern portions, and consists of mountainous and highland areas, with the rest being wide plains. The MODIS/Terra imagery, meteorological data for 16 April 2000 (DOY = 107) and DEM data outlining the changes of terrain, LUCC data depicting the different land cover are included in the analysis. The spatial resolution of the imagery is 1 × 1 km and overpass time is 10:50 h (local time). MODIS data includes land surface temperature, normalized difference vegetation index and surface emissivity. Meteorological data mainly includes the wind speed at reference height, sunshine duration, vapour pressure and daily maximum and minimum temperature. Spatial interpolation, re-sampling, projection transformation, mosaic and mask are successively performed using ENVI + IDL and MRT (MODIS Reprojection Tool) software. The flux algorithms were programmed using IDL (Interactive Data Language) development language.

RESULTS AND ANALYSIS

The red, near infrared and thermal infrared spectral data of MODIS are used to calculate r_0, T_s and *NDVI*. Figure 2 shows the r_0, T_s and *NDVI* imagery and their corresponding histogram distributions ((a)–(c), where frequency denotes the number of pixels). Statistics of Fig. 2 show that r_0 ranges from 0.02 to 0.21 with the mean value equal to 0.11 and T_s is from 279.04 to 312.38 K with the mean about 300.16 K and the range of *NDVI* is from –0.20 to 0.96 and the mean of *NDVI* equals 0.48. The value of r_0 is high in the east and low in the west spatially, which is contrary to *NDVI*. At the beginning of summer, the vegetation of the study area is primarily in the stage of growth period and mixed forests mainly distribute in the west, it is regarded reasonable that *NDVI* takes on a west–high–east–low spatial distribution and the range of *NDVI* is between 0.20 and 0.70. According to the classification scheme of the University of Maryland (http://edcdaac.usgs.gov/modis/mod12q1v4.asp), Land Cover/Change type is mainly the Croplands which accounts for 94% of the study area. Higher T_s is chiefly located in the area where Land Cover/Change type are Mixed Forests and Urban and Built-up. The range of T_s is from 290.00 to 305.00 K, which primarily presents the actual spatial distribution of the study area.

R_n, G and H of energy balance equation are obtained one by one with MODIS data and meteorological data, and LE is computed as the residual of energy balance equation and thereby E_d can be achieved with equation (11). The spatial distributions of R_n, G, H, LE and E_d, and their corresponding histograms are shown in Fig. 3. From the histograms, the R_n range of the study area is between 605.75 and 942.06 W m^{-2}, and the maximum, minimum and mean values of R_n for croplands are 886.25, 605.75, 751.28 W m^{-2}, respectively. G ranges from 12.94 to 100.26 W m^{-2}. The maximum G for croplands is 100.26 W m^{-2}, the minimum 12.94 W m^{-2} and the mean 72.25 W m^{-2}, H ranges from 0.01 to 821.97 W m^{-2}, in which crop areas having a maximum of 346.34, a minimum of 0.01, and a mean of 80.56 W m^{-2}; LE for the study area ranges from 0.15 to 817.39 W m^{-2}, where LE of the crop area has a maximum of 817.39, a minimum of 199.39, and a mean of 596.35 W m^{-2}. E_d of the study area ranges from 0.002 to 9.08 mm d^{-1}, where that of the crop area has a maximum of 6.74, a minimum of 3.79, and a mean of 4.31 mm d^{-1}.

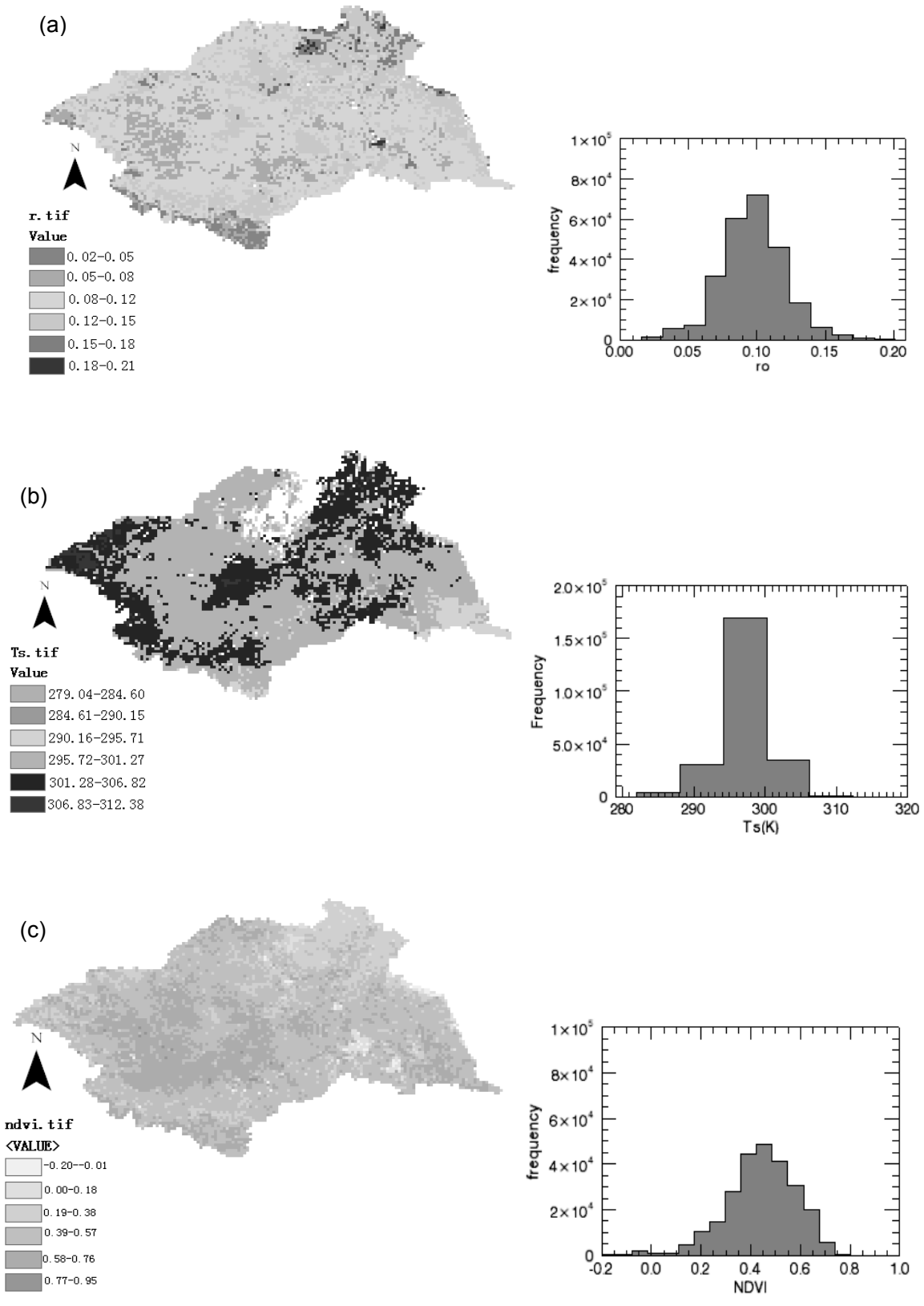

Fig. 2 The spatial distributions and histograms of (a) r_0, (b) T_s and (c) *NDVI*.

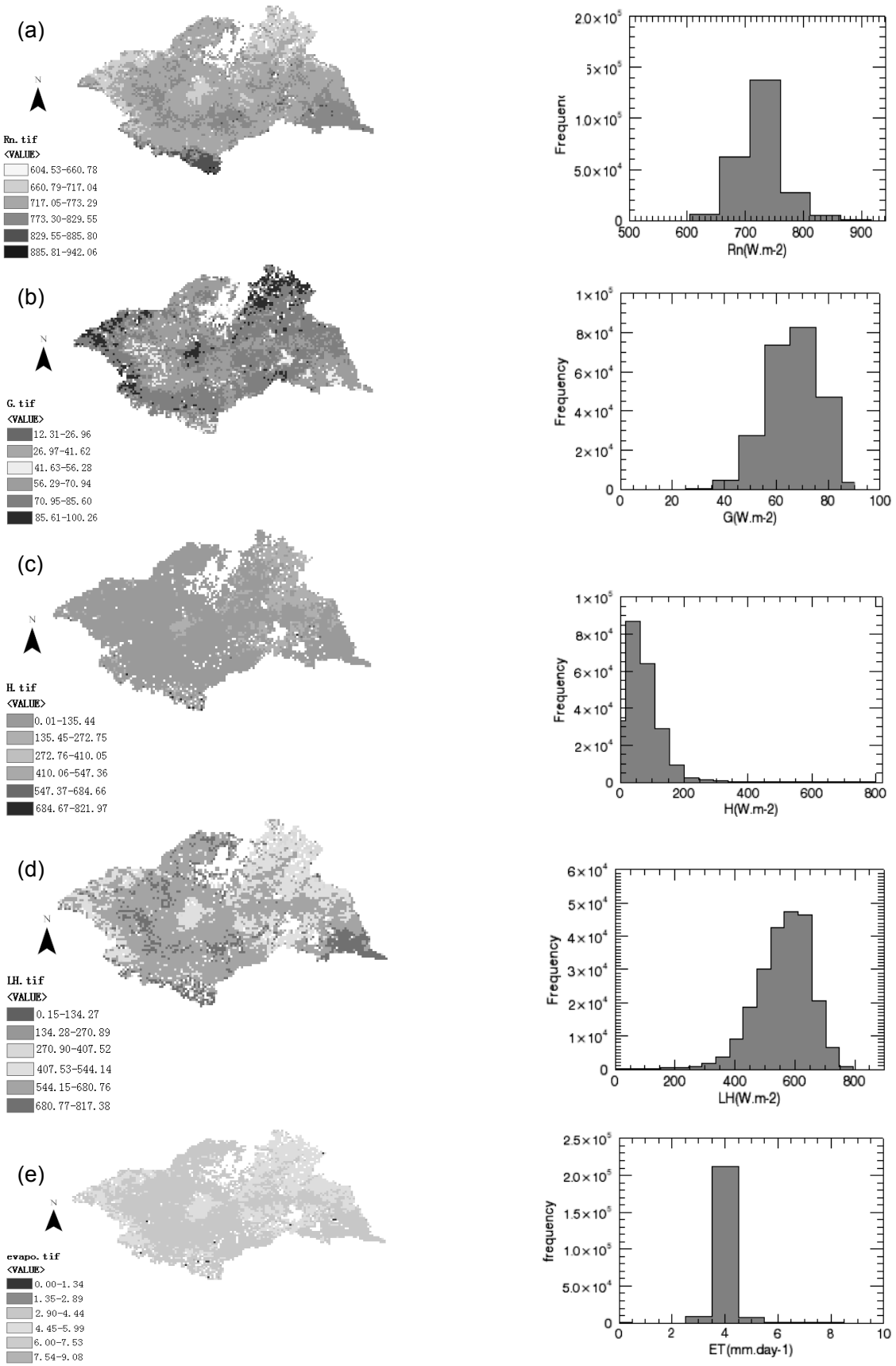

Fig. 3 Spatial distribution and their histograms of (a) R_n, (b) G, (c) H, (d) LE, and (e) E_d.

The southern part of the study area has a higher net radiation than the north in the spatial distribution. That is to say, the net radiation is higher at low latitude than high latitude, just as the sun radiation getting weaker from low to high latitude. Since R_n is determined by shortwave radiation and long wave radiation, when the surface properties of the study area doesn't vary a lot from the south to the north, and namely there are little variations to the long radiation from low to high latitude , in this way it can be regarded that the spatial distribution of R_n is reasonable. G has a very close relationship with T_s and r_0, and what can be seen from Figs 2(a) and 3(b) is that the spatial distribution of G is the same as that of r_0 on the whole, with an average of about 10% of that of R_n. As H is influenced by some quite complicated factors, its computation is simplified in this paper and it is higher in the east of the study area than in the west spatially, which is quite opposite to LE. The average of E_d at the study area is about 4.20 mm d^{-1},which is very near to the value 4.30 mm d^{-1} interpolated from the point observed ET by IDW, and it mainly ranges from 2.90 to 6.00 mm d^{-1}.

Eleven points observed ET and another nine of the observed ET at the study area are used to calibrate and validate the corresponding remotely sensed ET, respectively, when the instantaneous ET is converted to the diurnal E_d with equation (10). Results are shown in Table 1 ($\alpha = 9.08$, $\beta = -0.4097$). Table 1 indicates that the relative errors between observed ET and MODIS-based ET of five pixels, including Gan Yu, Shang Qiu, Dang Shan, HuaiYin, XuYi, are all less than 15% and four of nine pixels, including Bo Zhou, Dong Tai, Gu Shi, Huo Shan, the relative errors are higher because of the limited points observed ET that can be used for calibration in this study area.

Table 1 Comparison of the observed ETo and MODIS-based E_d (Unit, mm d^{-1}).

Pixel	Gan Yu	Shang Qiu	Dang Shan	Bo Zhou	Huai Yin	Xu Yi	Dong Tai	Gu Shi	Huo Shan
ETo	5.80	4.90	4.20	4.40	4.70	4.50	3.30	4.00	3.30
E_d	5.50	4.60	4.30	5.60	5.30	4.60	4.50	4.90	4.20

CONCLUSIONS

MODIS data, which is free and has higher temporal and spatial, and spectral resolution than previous NOAA-AVHRR, has been applied extensively in hydrology, water resources, meteorology and agriculture. This paper makes use of MODIS data and meteorological data to present the spatial distribution of ET at Huai River based on energy balance equations.

Results show that ET at the study area on the whole has a east–high–west–low trend. The calibrated sinusoidal relationship can improve ET precision of the study area compared to the uncalibrated sinusoidal relationship when we compare the observed ET with the MODIS-derived ET.

Where meteorological stations evenly distribute and the inversion parameters of remote sensing data have a higher precision, MODIS-based estimates of ET can primarily meet the basic needs. Considering the remotely-sensed sun radiation is higher than actual sun radiation, two calibration factors are introduced with the measured ET and the results are validated when the instantaneous ET is converted to

the diurnal ET. In the process of verification and validation, the mean value of 3 × 3 pixels including the observed "point" value is calculated as the pixel value to fit the remotely sensed value so as to improve the representation of the observed point data.

Simplifications have been performed during the retrieval of remotely sensed parameters and some empirical relationships still need to be verified with the observed data. There are still many problems in the process of calculation on large regions of spatial distribution of ET, such as the accuracy of parameters, scaling problems, and validation. All these problems mentioned above need further study.

Acknowledgements Support from the project of China National Natural Science Foundation (40671035, 50579053), the Special Fund of Ministry of Science & Technology, China (2006DFA21890) and the opening Research Foundation of State Key Laboratory of Hydrology-Water Resources and Hydraulic Engineering (2006412011), Hohai University is acknowledged.

REFERENCES

Ambast, S. K., Keshari, A. S & Gosain, A. K. (2002) An operational model for estimating regional evapotranspiration through Surface Energy Partitioning (RESEP). *Int. J. Remote Sens.* **23**(22), 4917–4930.

Bastiaanssen, W. G. M., Menenti, M., Feddes, R. A. & Holtslag, A.M. (1998) A remote sensing surface energy balance algorithm for land (SEBAL)-Formulation. *J. Hydrol*. **212–213**, 198–212.

Chen, J. (1988) A significant flaw and its improvement of remotely sensed evapotranspiration model in existence *J. Chinese Sci. Bull.* **6**, 454–457.

Choudhury, B.J., Idso, S.H. & Reginato, R. J. (1984) Analysis of an empirical model for soil heat flux under a growing wheat crop for estimating evaporation by an infrared-temperature based energy balance equation. *Agric. For. Met.* **39**, 283–297.

Guo X., Cai X. & Xin G. (2005) Analytical solutions of Monin-Obukhov length for stable surface layer. *Acta Scientiarum Naturalium Universitatis Pekinensis* **2**(41), 172–179 (in Chinese).

Huang, M. (2003) Advance of research on surface flux. *Arid Land Geogr.* **2**(26), 159–165.

Huang, M., Liu, S. & Zhu Q. (2004) Analysis of the factors impacting evapotranspiration estimation using remote sensing data. *Arid Land Geogr.* **27**(1), 100–105.

Liu, S., Mao, D. & Lu, L. (2006) Measurement and estimation of the aerodynamic resistance. *Hydrol. Earth System Sci*. **3**, 681–705.

Su, Z. (2002) The Surface Energy Balance System (SEBS) for estimation of turbulent heat fluxes. *Hydrol. Earth System Sci.* **6**(1), 85–99.

Wang, S., Chen, W. J.& Cilhar, J. (2002) New calculation methods of diurnal distribution of solar radiation and its interception by canopy over complex terrain. *Ecol. Modelling* **155**, 191–204.

Xie, X. Q. (1991) Estimation of daily evapotranspiration from one time of day remotely sensed canopy temperature. *Remote Sensing of Environment China* **6**(4), 253–259 (in Chinese).

Xingguo, Mo, Suxia, Liu, Zhonghui, Lin & Weimin, Zhao (2004) Simulating temporal and spatial variation of evapotranspiration over the Lushi basin. *J. Hydrol*. **285**, 125–142.

Zhang, R. (1999) Some thinking on quantitative thermal infrared remote sensing. *J. Remote Sensing for Land & Resour.* **1**, 1–6.